VLA SCIENTIFIC MEMORANDUM 146

A PROPOSAL FOR A LARGE, LOW FREQUENCY ARRAY LOCATED AT THE VLA SITE

R. A. PERLEY

National Radio Astronomy Observatory,

Socorro, N.M. 87801

W. C. ERICKSON

Astronomy Program, University of Md.,

College Park, MD. 20742

14 April, 1984

TABLE OF CONTENTS

1. SUMMARY

The diffraction-limited resolution of radio astronomical instruments has encouraged the development of interferometric techniques. The technique known as 'earth-rotation synthesis' has been utilized by numerous instruments (notably the VLA), and has proved immensely successful in providing full-field mapping of celestial radio emission with resolutions orders of magnitude better than that provided by the largest single antenna.

However, the use of earth-rotation synthesis has been almost wholly limited to centimeter wavelengths. At longer wavelengths, (λ > 1 meter), the only instruments which utilize the technique (the University of Maryland's TPT, and Cambridge's 151 MHz array) operate over limited (<5 km) baselines. There are two reasons why high resolution, low frequency interferometry has remained undeveloped. First, the very long baselines required to obtain useful resolution imply a prohibitive cost in transmission of the data to a correlator. Second, and more importantly, the disruptive effects of the ionosphere make calibration of the data very difficult on baselines longer than ~5 km. Recent hardware and software developments now enable serious consideration of a high resolution, low frequency instrument. The completed VLA waveguide system contains ample unused bandwidth for transportation of low-frequency astronomical signals over useful baselines, and new software techniques developed to improve the dynamic range of VLA data should enable calibration of low-frequency data taken from long baselines. It then becomes useful to discuss the technical and scientific aspects of a meter-wavelength synthesis instrument.

We propose that the NRAO construct a low-frequency synthesis array utilizing facilities already existing at the VLA site and operated in conjunction with the VLA. A useful array can be constructed for less than 1 million dollars, and would represent an excellent investment with regard to the science that will be returned. The array design and construction present no technological problems. We believe that data calibration can be accomplished using recently developed algorithms combined with a priori information on the sources in the field of view obtained at higher frequencies.

This report contains recommendations for the design of this proposed array. In examining various design options, we adopt the following constraints:

1) Operation of the low-frequency array should not displace or inconvenience the current VLA.

2) Maximum use should be made of the currently existing hardware and software at the VLA site, without violating the first constraint.

3) The total cost should be kept within reasonable expectations of what the NRAO RE (Research Equipment) budget can provide.

The proposed instrument will be a powerful tool for work on a broad range of astrophysical problems. The design beamwidth of ~ 10" - 20" at 75 MHz will resolve thousands of objects whose structures have never been studied at frequencies below 100 MHz. Chapter 2 lists examples of the types of projects which will become possible with this array.

Since the ionosphere is a turbulent and highly refractive medium, it strongly affects the propagation of low-frequency radio waves. Chapter 3 reviews the expected effects on the data and outlines the method of calibration we propose. In addition, the problem of non-coplanar baselines is considered.

The problem of calibration is described at length in Chapter 4. We show that a general solution to the calibration problem should exist, based upon the fact that the system noise is entirely determined by galactic emission in the field of view and not by the receivers. We show that for maps larger than $\sim 1^{D}$ in extent, there should exist sufficient flux density from background sources to allow calibration on the data, provided an approximate initial model of the stronger sources is provided.

We emphasize that these conclusions are based on certain ideas concerning the typical behaviour of the ionosphere. Tests are needed to confirm that the proposed method of calibration is actually practical. These tests can be made with elements of the 327 MHz system in the 'A' configuration and would be completed before any major expenditures are scheduled to occur. If the calibration is as simple as we anticipate (for a reasonable fraction of the total observing time), only modest computing facilities will be required. Because of these uncertainties, a detailed calculation of the required data analysis system will be deferred.

The proposed design is detailed in chapter 5. The proposed design can be summarized as follows:

1. Continuum capability at or near 75 MHz. Moderately wide-band antennas are recommended for frequency flexibility, both in order to avoid terrestrial interference and to allow bandwidth synthesis. Dual polarization is strongly preferred.

2. A maximum bandwidth of ~4 MHz (probably limited by interference), with two narrower bandwidths available. Attention should be paid to bandpass shaping to minimize confusion from sources outside the field-of-view.

3. An array consisting of at least 27 banks of antennas which will be permanently located near 'A' array stations. In addition, we propose to place banks with those VLBA stations within ~500 km of the VLA. The proposed array will operate only when the 'A' array stations are occupied by existing 25-meter antennas. The effective collecting area of each bank should be between 100 and 200 square meters. The banks should be equatorially mounted, and fully steerable. It is highly desirable to build more than 27 banks, since this will considerably reduce the severe aliasing problems that are expected.

4. Pre-amplifiers will be located at each bank so the signals can be conducted to the nearest VLA antenna with no significant loss in signal-to-noise. Further amplification plus frequency and bandwidth selection will be done at the VLA antenna. The signals will then be injected into the existing electronics for transmission to the control building.

5. At the control building, the signals will be extracted and recorded with a VLBA (or similar) recording system. These signals will then be played back into a special, dedicated correlator. A modest, dual-channel, narrow-bandwidth correlator is proposed. Multiple fields of view can be mapped by repeated passes of the data through the correlator.

6. Calibration and mapping will be done on a VAX, or equivalent machine, using currently existing self-calibration algorithms.

7. Presuming 27 banks with 2 MHz bandwidth and 8 hour integration with dual polarization, the expected rms noise at 75 MHz will be about 3 mJy, two orders of magnitude lower than any other system at this frequency.

Chapter 6 contains a rough estimate of the cost of our 'bare- bones' design. The array, including the correlator, can be built for ~$700K. Installation of antennas at VLBA sites to increase the angular resolution of

the system is estimated to cost ~$100K. In order to cover its fair share of the computing costs, we estimate that an additional $300K should eventually be budgeted for computer acquisition.

This will provide an array which will operate when the current VLA is in the 'A' configuration - approximately 3 to 4 months per year. A full-time array would cost approximately three times more. We estimate that approximately 5 man-years of technical labor are required to complete the array.

2. SCIENTIFIC JUSTIFICATION

The lack of instruments operating at meter wavelengths is by no means indicative of the scientific potential of this wavelength band. Until recently it has not appeared possible to build a useful low frequency instrument with arcsecond resolution. Now that methods to calibrate the data appear to exist, it is useful to contemplate the potential science.

In general, the potential results complement those which can be obtained by existing or planned instruments at centimeter-wavelengths. Compact cores and recent activity in galactic and extragalactic sources are best observed at short wavelengths; extended emission, halos, and evolutionary effects are best studied at long wavelengths. At these frequencies, synchrotron emission from old electrons is observed, electrons whose radiative lifetimes are usually so long that their energy spectra have not been modified by radiative losses.

The fact that long wavelength radiation interacts strongly with astrophysical plasmas is both a blessing and a curse. It means, for example, that free-free absorption will be observable in the vicinity of galactic nuclei and in the planes of some edge-on spirals, and that effects caused by interstellar and interplanetary scattering should be detectable. On the other hand, ionospheric refraction and scintillations make these observations difficult, and, as we have commented, have been responsible for the lack of high-resolution instruments in this wavelength band.

At long wavelengths, we also observe objects that radiate by coherent plasma proceses. Objects which possess dense plasmas and radiate by such processes - pulsars, flare stars, Jupiter, and the Sun - have very steep

spectra and strong polarization. It is likely that we shall eventually observe such radiation from dense extragalactic objects as well.

No planned or existing meter-wavelength instrument operates with a beam of less than ~1'. The number of galactic and extragalactic objects which can be usefully resolved increases dramatically for resolutions less than ~20". We recall that the Cambridge One-Mile Telescope's resolution of 20" usefully mapped hundreds of radio sources, revealing structures essentially unknown at the time, and that the initial Westerbork telescope synthesized a 20" beam. The instrument we propose will synthesize a 20" beam, or better, enabling projects that will be in no way inferior to those which have made the aforementioned instruments famous.

This chapter outlines some types of projects that we envisage for a high-resolution, low-frequency array.

2.1 Extragalactic Observations

1. Halos. The study of the large-scale emission found in and around individual galaxies and clusters of galaxies is best done at low frequencies, since this emission has a steep spectrum. As the electrons responsible for the emission diffuse outwards from their place of origin, they suffer radiation losses, and a spectral index gradient occurs. The resolution and frequency flexibility of the proposed array will be sufficient to study these effects. Such studies are needed in order to confirm the interpretation that some X-ray halos are caused by synchrotron emission. These studies are also fundamental to theories of cosmic ray origin.

2. Radio Galaxies and Quasars. These objects generally have low-brightness regions in which the spectrum of the radiation is steep, making low frequencies optimum for study of these regions. The radiation lifetimes

of the electrons in these regions are usually much greater than the radio source lifetime, so that observations at low frequencies will often reveal the source at the time when it was active in these regions. Such studies are essential in understanding the evolution of these objects.

3. Surveys and Serendipitous Discoveries. Most existing radio sky surveys have been made at low frequencies. From these surveys come both serendipitous discoveries and the lists of sources used for high resolution mapping at high frequencies. Serendipitous discoveries often provide the greatest opportunities for advances in our understanding of the physics in astronomical objects. An excellent recent example is the 6C survey discovery of the extraordinary radio jet in NGC6251. The proposed array will be an excellent survey instrument which can be 'expected' to uncover unexpected classes of objects. The array's sensitivity will be sufficient to allow source number counts in a frequency range where cosmological tests have not been attempted.

4. Studies of source variability at low frequencies. Some sources show significant variability at low frequencies, and the implied brightness temperatures often exceed the 'Compton limit' of $\sim 10^{12}$ K. Strong variations in 2145+067 have been reported at 80 MHz, revealing severe problems if the radiation is by the incoherent synchrotron mechanism. Recently, there have been suggestions that this low frequency variability is a result of slow interstellar scintillations, and not due to intrinsic source variability. This could be true for those sources that vary exclusively at long wavelengths, but not for those that vary coherently from centimeter to meter wavelengths. If the variations are caused by interstellar scintillation, their amplitude will vary as wavelength squared. Thus, 75 MHz combined with 327 MHz observations would quickly

distinguish between intrinsic and interstellar variation. High resolution observations are needed at long wavelengths because the compact, variable source component has a low flux density and is usually buried in surrounding non- variable emission.

5. Studies of the spectra of extragalactic objects. The synchrotron turnover frequency of compact objects supplies an estimate of the source size. The spectra of most galactic nuclei will turn over because of HII absorption, yielding estimates of HII contents and temperatures. These effects can be distinguished by their low frequency spectra.

6. Studies of normal spiral galaxies. The resolution of the proposed array will be sufficient to allow mapping of the low-frequency, non-thermal emission of hundreds of spiral galaxies. Data concerning any halos of such galaxies are crucial to problems of cosmic ray acceleration and storage. In this respect, determination of the thickness of the synchrotron-emitting layer in edge-on spirals is particularly important. Observations of relatively distant spirals may be more rewarding than these of large, nearby spirals such as M31 because the emission from smaller angular diameter spirals should be less confused by fluctuations in the foreground emission of our own Galaxy.

2.2 Galactic Observations

Previous low-frequency observations of the galactic plane could not separate its general emission from that of the interesting individual components located within the plane. Again, we emphasize that as the resolution of an instrument exceeds ~20", a veritable host of objects can be studied. These include both coherent and incoherent radiators. Examples of projects include:

1. Supernova Remnants: Supernova remnants throughout the galaxy will be well-resolved by the proposed array. We expect to observe radiation from the electrons accelerated by any precursor shocks ahead of the normally-observed supernova shock. Young, filled center SNRs show spectral index variations which probably are related to electrons accelerated in the early stages of the explosion and those accelerated at the shock front. We should be able to distinguish these two populations.

The VLA maps of Cas A display a wealth of detailed structure at 6 and 20cm. It will certainly be useful to obtain high resolution maps at 4 m wavelength for comparison with these data. This will disentangle thermal and non-thermal emission. One should also search for any steep-spectrum compact object in Cas A, i.e. the compact object that has been reported with VLB and IPS observations at decameter wavelengths.

2. Pulsars. Fast, highly dispersed pulsars (such as the millisecond pulsar) located anywhere in the Galaxy would be observable as compact continuum sources.

3. Galactic center. The galactic center is quite strongly absorbed by HII at 75 MHz, but it should still be easily observable with this proposed system. The compact source at the galactic center might well generate coherent, long wavelength radiation.

4. HII regions. At these frequencies, virtually all HII regions will be optically thick, allowing a direct measure of their temperature.

5. Flare Stars. Flare star observations should prove fruitful. By analogy with the Sun, we would expect that the centimeter wavelength emission from flare stars is generated by a different mechanism from the meter wavelength emission. In this respect, it will be very advantageous to observe at 4 meter, 1 meter, and centimeter wavelengths simultaneously to

determine to what extent solar analogies hold for other classes of stars. This will assist our understanding of both stellar and solar radiophysics.

6. Star Clusters. The wide-field capability achievable by reprocessing tape recorded data is a distinct advantage. An entire large angular diameter cluster of stars can be observed simultaneously with the proposed system. For example, the entire Hyades cluster - so important to the cosmic distance scale - could be observed at once, whereas only one star can be observed at one time at 20 cm.

7. Galactic background emission. Historically, long wavelength observations of the Galaxy have found structure down to the limiting resolution of each instrument that has been employed. Assuming that the interstellar medium is turbulent, that it is pervaded by strong shocks, and that it possesses several phases, we might expect that its synchrotron radiation would display small-scale structure. If so, the physical interpretation of such structure would be of considerable interest.

Low frequency recombination lines might be observable via stimulated emission or absorption mechanisms. The calculation of these stimulated effects is based upon many poorly determined parameters of the interstellar medium, but these predictions suggest that the 60-90 MHz frequency range is a transition range for recombination lines. The lines are predicted to be in absorption below 50 MHz, and in emission above 100 MHz; their contrast may be very low in the 75 MHz region.

8. Interstellar propagation effects. The ionized component of the Galactic plane strongly affects the propagation of radio waves through it. As the array will be able to identify large numbers of background radio sources seen through the plane, it should be possible to find ones that are behind dense HII regions. Scattering effects in the HII regions will permit

a determination of the small-scale turbulence in these plasmas. Relatively cool, dense plasmas also cause appreciable absorption if they contain even moderate numbers of free electrons.

9. Exotica. Low frequency, high resolution observations of exotic objects like SS433 would certainly be revealing.

2.3 Solar System Observations

The objects in our own solar system radiate meter-wavelength radiation by both coherent and incoherent mechanisms. Potential scientific projects include:

1. The Sun. Of the four frequencies available with the Culgoora radioheliograph, 80 MHz produced the most useful data. This is due to the wide diversity of intense solar emissions that occur below 100 MHz. Many of these bursts occur near the plasma level, and in propagating out from this level, the radiation is subject to considerable coronal scattering which probably smears out features less than one or two arcminutes in size. In most cases, we may not add much to the existing lower resolution (3-4 arcminute) data. However, the sun occasionally ejects a synchrotron-emitting plasmoid (moving Type IV) source which travels many solar radii above the plasma level where coronal scattering is negligible. These ejections are associated with a great variety of important interplanetary and geophysical phenomena. It will be important both to plasma physics and to solar-terrestrial physics to study the detailed brightness distributions of these plasmoids. Once again, the use of tape recorded data will be advantageous; moving Type IV sources can be tracked throughout the corona simply by reprocessing the data to follow their movement.

The sun occasionally produces rapidly varying (10 to 100 millisecond) bursts. These must originate in small angular diameter regions or else

scattering would wash out their temporal variations. The proposed array could conceivably be equipped with a fast mode to observe such phenomena.

2. The Planets. Most planets emit only thermal radiation, which is best studied at short wavelengths. However, the radiation belts of Jupiter subtend an angle of ~4.5 arcminutes and radiate synchrotron emission. Long wavelength observations of these belts combined with short wavelength observations will yield the spectrum of the radiation belt electrons. Such spectral observations would be particularly important when combined with Galileo observations.

If the proposed system were equipped with a fast mode of data recording, it could also be used to search for electrostatic discharge radiation from Saturn.

The moon would be, at least, amusing to observe with the system. It should appear as a large, dark hole in the galactic background. Conceivably, it might be used as a sidelobe free (negative) 'beam' with which to calibrate galactic background intensities.

3. Solar Wind Turbulence. Observations of the phase and frequency scattering of monochromatic spacecraft signals show that the inner scale of the turbulence in the solar wind is $\leq$ 5 km. Clark Lake observations of the scattering of discrete sources show this scale is >2 km. The proposed array would bridge the gap and give a definitive measurement of the scale lengths and the shape of the turbulent, solar wind structures. Appreciable scattering would be expected whenever a source is observed within 10 to 15 degrees of the sun.

In summary, we believe there are many astrophysical problems which can be addressed with a low frequency instrument. Such an instrument could be

used for exciting new research in almost all fields of astronomy. We are confident that the scientific rewards in opening up a new frequency range to resolutions currently unattainable will be great.

3. PROBLEMS IN CALIBRATION AND MAPPING AT LOW FREQUENCIES

In this chapter we identify the major problems expected to affect data calibration, and outline the proposed solution. The non-coplanar baseline problem is expected to be significant in low-frequency synthesis - this problem and its proposed solution are detailed.

3.1 Atmospheric Effects

Refraction effects in the atmosphere have a strong influence on radio astronomy. The notable effects are a net bending of the ray and a change of the phase due to the altered path length combined with the change in the index of refraction. If the Earth's atmosphere were horizontally stratified, interferometry from the Earth's surface would be relatively straightforward, and knowledge of the vertical atmospheric profile would be sufficient to allow a priori corrections for all atmospheric effects. Unfortunately, the atmosphere is not smooth in general, and effects of small scale irregularities are important.

The effect of the neutral atmosphere to low frequency interferometry is entirely negligible. The index of refraction in the neutral atmosphere is independent of wavelength, so the effect on interferometer phase is inversely proportional to wavelength. Extrapolating the phase perturbations measured at centimeter wavelengths with the VLA to 4 meters shows that the neutral atmospheric irregularities contribute at most a couple of degrees of phase.

Much more important is the effect of the ionosphere. The path change introduced by the presence of an ionized medium is (in MKS units)

$$\Delta L = -4.5\times10^{-16}\lambda^2 \int n dl$$

where n is the electron number density, and the integral is along the ray path. The total electron content is typically $10^{17} m^{-2}$, with fluctuations of a factor of ten each way. This gives a typical extra path of ~720 meters at 75 MHz. Although the ionosphere is less than 0.01% ionized, this is sufficient to make its refractive effects dominant over those of the neutral component at meter wavelengths. Both the smooth and irregular components of the ionosphere are important, and we discuss each separately.

3.1.1 Effects of the Smooth Ionosphere

A practical definition of the smooth ionosphere is that its effects are, at least in principle, calculable and correctable. This implies that the vertical gradients are known, so that analytic methods will produce the desired quantities. In what follows, we assume this to be true.

The total bending can be calculated relatively easily, and will not be important to low frequency astronomy because the only effect of the angular error is to necessitate a correction in the antenna pointing. The expected bending at 75 MHz is a few arcminutes at most, while the primary beam will be at least 20 degrees.

More important is the effect on the interferometer phase. The total phase introduced by the ionosphere is enormous - typically 1000 radians at 75 MHz at the zenith. Diurnal differences in total ionized content make these values change daily by a factor of ~3, with most of the change occuring just before sunrise and after sunset. However, the effect of the smooth ionosphere on the phase of an interferometer is much less than the total phase change since this change is nearly the same to both antennas. In a stratified ionosphere, the largest effect on the interferometer phase is caused by the effective difference in the source elevation between the two antennas. The resulting difference in phase can be calculated from the

ionospheric profile. Assuming a uniform profile to simplify calculations and to provide reasonable estimates, we expect the interferometer phase change due to the smooth ionosphere on the longest VLA baseline at 75 MHz will be ~5 tan(Z)sec(Z) radians, where Z is the zenith distance. As this quantity is time-variable, it may not be possible to exactly correct the phase, especially not in real time. However, the largest part of it, due to the mean content typical for the time of day, can be removed with an accuracy estimated by Hinder and Ryle (MNRAS 154, 229, 1971) of about 20%. This is certainly not sufficient to enable good mapping, and a better correction method must be found.

The ionosphere also causes a strong rotation in the plane of polarization of an electromagnetic wave. Typically, the plane of linear polarization is rotated by 10 radians at 75 MHz, with a λ^2 dependence. The differential effect across a 35 km interferometer aperture is quite small and should not render polarization measurements impossible. However, the time-variability of the total rotation means that if any sources are linearly polarized at these wavelengths, circular polarization must be presented to the correlators to ensure that the system's response is not time variable.

Circular polarization is also necessary if we wish to couple VLBA 'out-stations' some hundreds of kilometers away into the system. Over such baselines, differential Faraday rotation could be many radians.

The apparent change in baseline length caused by differential refraction is negligible at these frequencies and baseline lengths.

3.1.2 The Effects of the Irregular Ionosphere

As is the case in the neutral atmosphere, the ionosphere shows irregularities on many scales, both in time and space. And as in the case

for the neutral atmosphere at centimeter wavelengths, the effects of the irregularities on an interferometer are of paramount importance. Although the irregularities change the total electron column density by less than 1%, this is enough to cause phase irregularities of many radians to appear on meter wavelength interferometers.

The effect of irregularities in the ionosphere upon the radiation field as measured on the Earth is commonly looked at from a diffraction viewpoint. Considerable work done in the 1950s showed that the irregularities act as a thin phase-changing screen. If the phase changes are less than ~1 radian, then the spatial baselines on the ground is the same as that of the irregularities themselves. At the frequencies of interest for the proposed array, this condition is usually met. The correlation scale upon the ground is important because it determines the type of calibration which must be used. If the scale is smaller than the interferometer scale, antenna based calibration will be necessary. Irregularities are known to exist on scales as small as 1 km, so it is clear that if we are to observe during these conditions in the 'A' configuration, antenna based calibration is necessary. Even if we are to restrict observations to conditions in which the irregularities are of 5 - 20 km scale, antenna-based calibration is still required.

The typical scale size of ionospheric irregularities generates two different scales of interest to low-frequency observations. The first is the angular scale, as seen from the ground, over which a particular antenna calibration will be valid. This angle will be called the isoplanatic angle. It is of especial importance because it will ultimately limit both the map size and the angle over which calibration of an antenna can be accomplished. The second scale is the temporal scale over which changes occur to the

antenna phase. This scale can be calculated from the isoplanatic angle, the height of the ionosphere, and the velocity of the irregularity.

We can classify the ionospheric spatial irregularities into three scales. The largest scale is ~1000 km, and moves with velocities ~500 m/sec. Not only is this scale rather rare (existing only during magnetic storms), but it is of no real significance to interferometry because the angular scale seen from the ground is about 45°, and the corresponding temporal scale is over 30 minutes. This combination of scales makes regular calibration straighforward.

The next smallest, and the most common, scale occurs between 40 and 160 km, with speeds of 100 to 200 m s^{-1}. The corresponding angular and temporal scales are 5 to 20 degrees, and 20 minutes. This scale will restrict normal calibration (especially at the small end) as strong, unconfused calibrators are typically 10 degrees apart. The time scale of 20 minutes presents no problem provided the phase excusions are moderate. As outlined below, and expanded upon in chapter 4, we believe we can easily calibrate this scale by using the sources available within the $\sim 5^{\circ}$ window alone.

The smallest scale is that set by scintillations. This phenomenon produces rapid (~30sec) amplitude and phase fluctuations, and is associated with small scale (~1-5 km) fluctuations in the ionized number density near 400 km height in the ionosphere. It is primarily a night-time phenomenon, and is most common at both high and low magnetic latitudes. It is especially notable at frequencies below 40 MHz, and is not expected to be a dominant phenomenon at the frequencies we are considering. Nevertheless, it is useful to contemplate whether we could calibrate the array during such activity. The angular scale is less than 1 degree, so there are very few

strong background sources available for calibration. However, as we shall show in the next chapter , there remains enough flux density even in this small a region to believe that calibration can be done, providing a suitable model of the region is available.

Data concerning the stability of the ionosphere over spatial sizes of tens of kilometers and temporal scales of tens of seconds to minutes is, at best, fragmentary. There exists extensive literature concerning the geographic and temporal variations of maximum density, but very little about scale size variations. The scale sizes are not well correlated with ionospheric densities; in fact, it is well known that scintillations reach a diurnal maximum near local midnight, when the density is approaching minimum, and they may also reach a secondary maximum near local noon, when the density approaches maximum. Seasonal and solar cycle variations of scale sizes are not well documented. Scintillation activity is known to be intense in the auroral zone and in the region of the equatorial electrojet, but at mid-latitudes it appears certain that the ionosphere will be stable enough to permit operation during some fraction of the time. Seasonal or solar cycle variations in the operating conditions may well exist, but we do not expect them to be of dominant importance.

In the 1970-73 period, a series of VLBI experiments at 74 MHz yielded fringe patterns that were normally stable to about 0.5 radians over baselines of 50 to 2000 km, and time scales of ~100 sec. This agrees with experience at Cambridge and Westerbork. Recent 81 MHz long-baseline interferometry by Hartas et al. (MN 205, 625, 1983) on baselines up to 1000 km have shown good results. Using 100 sec integration, they suffered decorrelation due to scintillation of less than 4% under normal conditions. Only occasionally was there complete loss of correlation, and this they

ascribe to abnormal ionospheric conditions. On the other hand, some Jodrell Bank data at 408 MHz shows phase deviations of 10 to 20 degrees for sources separated by only 20 to 30 arcminutes. Ooty observations at 327 MHz commonly show scintillations, although it is probable that this phenomenon is associated with the equatorial electrojet, and will not be a problem at our latitude. It is imperative that we obtain more 327 MHz data over 20-30 km baselines in order to predict the performance of a 75 MHz system. Limited observations (a few hours) with a 20 km baseline at 327 MHz at the VLA have shown phase variations of 10 to 50 degrees with timescales of 10 to 50 minutes. No evidence was found for time scales less than 2 minutes.

Whatever the distribution of scale sizes is, our planned mode of observing will be to throw away data which is corrupted sufficiently badly as to render calibration difficult or impossible. The best way to determine the quality of data is to observe strong sources lying within the antenna beam. We plan to tape-record the antenna signals, so that those days of very good observing conditions can be fully processed while those corrupted by turbulent ionospheric conditions can be purged. The only really effective way to remove ionospheric effects is to observe simultaneously on two or more frequencies sufficiently widely spaced to give significantly different interferometer phases. This, however, is only effective if the visibility phase is unchanged over the frequency range, a condition unlikely to occur in practice except for strong, isolated point sources. A much better reason to contemplate two-frequency observations is that this will allow bandwidth synthesis - an effective doubling of the information. We will discuss this point in more detail in Chapter 5.

The calibration problem as a whole is the same as for the current VLA. We expect the antenna phases to vary by radians over scales of a few

kilometers, with temporal scales of minutes. Because the angular scale of irregularities is of order, and often less than, the mean separation between unconfused calibrators, we believe self-calibration techniques must be employed, using as signal the flux density lying within the isoplanatic region.

3.2 An Outline of Calibration

For the reasons detailed in Chapter 3.1, we must employ self-calibration in mapping at low frequencies with high resolutions. We can discern two cases:

1) A strong source dominates the total flux density from within the isoplanatic patch. In this case self-calibration can recover the antenna gains in exactly the manner used now for data taken with the current VLA. All that is required is a reasonable initial model. If the strong source is unresolved, the initial model is simply a point source. If the strong source is well resolved, a model made from another low frequency (say, 327 MHz), should suffice as an initial guess. In either case, calibration should be relatively straightforward.

2) In the absence of a strong source, we feel that self-cal can still provide the calibration parameters if the total flux density from the background sources located within the isoplanatic patch exceeds the system noise. This will normally be the case. Provided adequate signal/noise is available, a reasonable model of the brighter background sources lying within the isoplanatic patch will serve as a slightly more complex example of calibration on an extended source. Again, we feel that a 327 MHz map will provide the model if no other information is available.

The important question is what constitutes an adequate signal-to-noise ratio (S/N) for self calibration to succeed. The signal is the modelled

flux density, while the noise originates both from the thermal fluctuations and from the effects of unmodelled background sources. The important parameter is the S/N on a single baseline, since this is the raw data seen by any calibration algorithm. As the noise fluctuations are random to each baseline (whether they are due to thermal noise, or to background confusion), the net S/N available for any one antenna gain solution will be $\sqrt{N}$ times better than on any single baseline, where N is the number of antennas available for the solution. We expect to use the longer spacings preferentially for solutions, so that N will be about 16 to 25. Thus, the net S/N will be ~4 times better than that available on a single baseline. We also believe that a net S/N of ~5 should be sufficient for calibration to succeed; certainly 10 will be more than adequate. Thus, the baseline-based S/N should be at least one, and preferably ~3.

An observing scenario is then as follows: The region of interest is tracked for a full 8 hours. The antenna signals are recorded on tape. The correlator will monitor the phases of the strongest one or two sources in the primary antenna beam. If these data indicate the ionosphere is in too disruptive a state to expect useful data, the data will be purged. If the data are considered acceptable, correlation for the field of interest will be done, with calibration done on a computer of the VAX class using algorithms similar to those now in common use. The model will be provided by a map of the region at a nearby frequency (most likely 327 MHz). If the data is of very good stability, further processing of the recorded signals will be done for other interesting fields of view.

Further analysis of the SNR problem is presented in Chapter 4.

3.3 The Non-Coplanar Baseline Problem

Use of the 2-dimensional FFT for map making implicitly assumes there is a two-dimensional relation between the visibility measurements and the sky brightness. This is not exactly true. The phase measured by a phase-tracking interferometer is (subject to the approximation that the field of view is much less than a radian):

$$\phi = 2\pi(u\ell+vm-w\theta^2/2)/\lambda$$

and is thus a function of the three baseline components, u, v, and w, the source coordinates with respect to the phase tracking center, ℓ and m, and θ, the angular displacement from the phase tracking center. The interferometer measures the visibilities in a three-dimensional volume and not, as is commonly assumed, in a 2-dimensional plane. Note that the effect is quadratic in angular displacement, so that low frequency observations with their large primary beamsizes are more likely to be affected. For E-W interferometers, a convenient transformation exists which allows a 2-D grid to be used. This convenient solution cannot be utilized for the VLA.

The effect of the w term can be calculated for 75 MHz by assuming the maximum delay will be about 20 km. The error term $\pi w\theta^2/\lambda$ reaches 1 radian at an angular displacement $\theta = 30'$. This will often be smaller than the angular field of view as limited by ionospheric effects, and greatly less than the primary beam field of view. If the simple 2-dimensional transform is to be used without complications from sources outside ~30', the signals from these sources must be suppressed. The obvious way to do this is by utilisation of the bandwidth and time-averaging effects. An angular field of 30' corresponds to a bandwidth of about 1 MHz, and time averaging of three minutes. Both of these are quite practical, so it appears that the coplanar baseline problem can be avoided by limiting mapping fields of view of less

than 1°. This corresponds to map planes of $\leq 1024 \times 1024$ cells.

Should we wish to synthesize larger fields of view, (presuming the isoplanatic region allows this), there are two accepted methods which can deal with the problem. They are:

1) Use of 3-D transforms. Barry Clark has outlined the procedure in the Synthesis Mapping Workshop. The final map is extracted from a curved surface in the three-dimensional map. The result can only be cleaned with great difficulty as the effective beam changes over the map.

2) Use of mosaics. A number of small maps are made covering the total field of view. For each small map, the 2-D transform is valid. The maps are simultaneously cleaned using the Clark formulation of CLEAN. The Fourier transform of the components are subtracted from the ungridded data, allowing the maps to be cleaned to the edges, and the effects of sidelobes of any one source to be removed from all sub-fields. This method is implemented in the AIPS task MX, and is generally very effective.

4. SENSITIVITY, CONFUSION AND NOISE

Radio telescope parameters at meter wavelengths are very different from those commonly encountered at centimeter wavelengths. In this chapter we describe the contributions to the system sensitivity and noise. Detailed calculations are given in the Appendices. Since self-calibration is essential to the operation of the proposed array, these calculations are necessary to delineate the conditions under which calibration can succeed. These conditions are then needed to set the system design.

4.1 System Temperature

At meter wavelengths, the background sky temperature is dominated by the emission from our own galaxy. Low resolution observations have shown that the sky temperature at galactic latitudes $|b^{\prime}|>10^{\circ}$ is ~20K at 408 MHz. With a flux density spectral index of α, the sky temperature at a lower frequency can be expressed as

$$T_{sky} = 20(408/\nu_M)^{2+\alpha}$$
$$= 20F^{2+\alpha}$$

where $F = 408/\nu_M$ is a normalised frequency parameter and ν_M is the frequency in MHz. At 75 MHz, the sky temperature is 2100K, using $\alpha = 0.75$. Since typical receiver temperatures are much less than this, it is clear that the system temperature will be dominated by the contribution from the average galactic background. This situation is in contrast to that normally encountered in radio astronomy where the system temperature, and hence the sensitivity, are set by the receiver noise.

As we can then assume the noise is set by the sky background, it is straightforward to calculate the thermal noise per baseline. This is shown in Appendix A to be:

$$\sigma_t = 50F^{2+\alpha}A_e^{-1}(B_M t)^{-1/2}$$

In this expression,

σ_t = the rms noise per baseline in Jy.

$F = 408/\nu_M$,

ν_M = the frequency in MHz,

B_M = the bandwidth in MHz,

A_e = the antenna effective collecting area

t = the integration time in seconds.

In terms of the antenna main beam solid angle, the thermal noise per baseline is, using $\lambda^2 = A_e\Omega_M$:

$$\sigma_t = 90F^{\alpha}\Omega_M(B_M t)^{-1/2}.$$

The solid angle, Ω_M, is in steradians, and the other symbols are defined above.

4.2 Confusion Noise and Signal

At low frequencies, an important source of noise can be the interferometer response to background sources lying outside the field of view. The very large number of background sources involved allows an analysis by random-walk techniques. Here we give the essential results of this analysis. The details are relegated to Appendices A and B.

The analysis is considerably complicated by the practical question of separating 'signal' from 'noise'. In keeping with our requirement that calibration must be done on the sources within the isoplanatic region, we have defined as 'signal' the N sources of greatest flux density lying within this region. These N sources contribute a fraction, f, of the total flux density available within this region. The effects of all other sources within this region, plus all sources lying outside it, are considered 'noise'. The analysis of Appendix A is summarized in Table 1:

Table 1.

Flux Density (in Jy) Available for Calibration at 75 MHz

f	F_{mod}	F_{min}	N
1.0	9.8Jy	.0036Jy	167
.75	7.3	.12	10.2
.50	4.9	.91	2.0
.25	2.5	4.0	0.25
.10	1.0	14.2	0.04

In Appendix A it is shown that at 75 MHz we should expect the total source flux density per square degree to be 9.8 Jy. In the Table, the first column represents f, the fraction of this total which we intend to use for calibration. This fraction is multiplied by 9.8 to give the actual total flux density used for modeling shown in the second column. The flux density of the weakest source needed for modeling is given in the third column, and the fourth column gives the number of sources per square degree which must be modeled.

In comparing the first and third rows, it is noteworthy that we need only to model two sources per square degree in order to obtain half the total flux density. This gives us reason to believe that a simple model, comprising only a few sources and half of the available flux density, would provide the needed signal for calibration.

The calculation of 'confusion noise' follows from the same analysis. There are two contributions: the first arises from unmodeled sources in the field of view, the second from all sources rumbling through the sidelobes. The analysis of Appendix A shows that if we model 50% of the flux in the field of view, use square bandpasses and box-car time-averaging, the rms noise due to the passage of background sources is:

$$\sigma_c = 66F^{\alpha}(\nu_M B_M t)^{-1/2}.$$

In deriving this ratio, we have assumed that the field-of-view is equal to or less than the isoplanatic patch size. The ratio of thermal to confusion noise is $0.75F^2\nu_M^{1/2}/A_e$. At 75 MHz, this ratio becomes approximately $200/A_e$, and is less than one for practical bank sizes. This indicates that thermal noise due to the galactic background emission will dominate. However, the ratio is only slightly less than one, meaning that some attention should be paid to bandpass shapes, and perhaps to non-box-car averaging as a means of rejecting confusion noise.

4.3 Signal/Noise Ratio

It is now straightforward to calculate the signal-noise ratio. The signal is assumed to come from the strongest of the available sources totalling a fraction f of the total flux density, and the noise is the thermal noise due to the galactic background (this presumes that some degree of design has gone into the bandpasses). It is assumed that we are far from the galactic plane. (In the galactic plane, the source and confusion effects and statistics may be different and the thermal noise level will certainly be higher. This case has not been treated in detail.) The result is:

$$SNR = 100f(B_M t)^{1/2}\Omega/\Omega_M.$$

Here, Ω is the field of view used for modelling, while Ω_M is the bank main beam solid angle. The field of view will be set by the bandwidth and time-averaging effects. Assuming this is equal to or less than the isoplanatic solid angle, the SNR becomes:

$$SNR = 2.5\times10^{-3} f A_e \theta_{iso} \nu_M^{3/2}.$$

The field of view θ_{iso} is the angle over which the phase perturbation due to the ionosphere is much less than a radian, or the mapping field of view, whichever is smaller.

This expression can be inverted to calculate the required bank area sufficient to allow calibration. The minimum size, for 50% modeling, and SNR of ~1 at 75 MHz is about 75 m^2, for angular scales of ~1°. A safer level is signal-to-noise of three, for which banks of approximately 200 m^2 will be required. Relaxing the angular scale constraint to larger angles will certainly allow calibration with smaller banks; however, it must be considered useful to plan a margin of error, and for this reason, we prefer to utilize bank effective collecting areas of more than 150 m^2.

5. ASPECTS OF ARRAY DESIGN

The previous two chapters dealt with the expected problems attending observing at meter wavelengths over long baselines. We concluded that the data can be calibrated by employing self-calibration algorithms with model information of the field of interest. This strategy places various constraints on system design, most particularly on the bandpass shapes, bank size, and number of banks. In this chapter we will discuss the proposed array design.

This chapter is divided into two main parts. The first deals with the global system parameters such as frequency, bandwidth, polarization and antenna placement whose selection are influenced largely by astronomical constraints. The second presents the component design constraints which we feel are set by the global parameters. This latter discussion starts with the antennas and essentially follows the signal path through to the correlator and data processing. We attempt to identify potential problems of each component, but will not identify complete solutions. This chapter is intended mainly to be a notebook in which expected problems and possible solutions are briefly mentioned. We feel that it will represent an adequate start to actual engineering of the various components.

5.1 Global Parameters

5.1.1 Frequency

The preferred frequency of operation lies between 50 and 180 MHz. The low-frequency system currently being installed on the VLA will operate near 330 MHz, so contemplation of a frequency above ~200 MHz appears unnecessary. Below 50 MHz, a combination of decreasing resolution and increasing ionospheric problems seems to reduce the scientific and technical

viability. We initially set a frequency near 75 MHz as the primary design frequency.

The reasons for operation in the 75 MHz range are as follows:

1) It represents a step from 327 MHz similar to the ratio between L, C, and U bands.

2) The new 151MHz telescope is in operation at Cambridge (although with only a 5 km baseline).

3) Radio astronomy has no protected band in the U.S. between 75 and 327 MHz, while there exists an exclusive band between 73.0 to 74.6 MHz.

A necessary precursor to any final selection of band is a complete RFI monitoring program over the band from 50 MHz to 200 MHz. This should be started as soon as possible. There has been preliminary monitoring between 68 MHz and 200 MHz. This shows that there is little variation in the RFI spectrum from day to day, and typical results are shown in Figs. 1, 2 and 3. Preliminary conclusions are:

1) Between 68 and 88 MHz, the RFI spectrum is dominated by television. Between the channel allocations, considerable interference-free regions are available - with bandwidths up to 4 MHz. The region between 68 and 72.5 MHz is especially clear, while the region near the allocated radio astronomy band contains moderate level signals. It appears that initial observations might be centered near 70 MHz. Good filters will be needed to reject the nearby television signals.

2) The region betwen 88 and 175 MHz is heavily used by FM radio and communications. The only relatively interference-free region seems to be from 113 to 116 MHz.

3) Above 170 MHz, the situation improves as the presence of the television bands discourages competing communication. There appears to be

~4 MHz available near 173 MHz, plus other 2 to 5 MHz bandwidths available at higher frequencies.

The RFI will not improve in the future, but unless unfortunate developments occur in the vicinity of the VLA (high power transmitters, high voltage power lines, etc.), the RFI spectrum should not significantly deteriorate. It is extremely important that the system be easily tunable over a range of at least 20 MHz. This capability will allow best future use of interference-free bands, and the possible use of bandwidth synthesis.

5.1.2 Bandwidth

It seems likely that interference will restrict the bandwidths to 5 MHz or less, probably 1 to 2 MHz. As discussed in Chapter 3, these bandwidths correspond with the largest sky area that can be mapped without serious distortion by 2-dimensional transforms, and still allow calibration based on the stronger sources lying within the region limited by the bandwidth effect.

As discussed in chapter 4.2, it will be useful to use bandpass shapes which will limit the inclusion of background sources passing through the sidelobes. This requires bandpass shapes with smooth edges like an exponential. Since such functions contain extensive skirts, our susceptibility to interference will clearly increase. Ideally, we would like to have both interference rejection and rejection of sources outside the mapping area. A seemingly reasonable compromise would use an optimum shape (from the point of view of background supression) down to the ~-20db level, then have the skirts fall off sharply for interference rejection.

Clearly, a choice of bandwidths will be useful, as the interference spectrum is highly variable. A suggested range of bandwidths are 4, 2, and 1 MHz.

5.1.3 Polarization

Circular polarization must be presented to the correlators due to the expected temporal change in the ionospheric Faraday rotation of any linearly polarized signal. The typical ionospheric Faraday rotation at 75 MHz is ~10 radians, with variations of factors of two or more from night to day. However, this does not mean that linear polarization capability must be rejected. As the horizontal gradients in total electron content are less than ~1% over scales of tens of kilometers or more, we anticipate differential Faraday rotation across the array of less than 0.1 radians. Linear polarization mapping with the VLA-based banks alone is feasible, provided that the total rotation can be removed. However, over the longer baselines, from the VLA to Pietown or Los Alamos, the differential Faraday rotation is expected to be large.

We do not regard linear polarization capability as a high priority, simply because there is currently no evidence for linearly polarized synchrotron emission at these low frequencies. It would be better to wait and see if the 330 MHz system demonstrates the presence of significant linear polarization from radio sources before including the capability into the 75 MHz system. On the other hand, no design step should be taken which will later exclude the possibility of full polarization mapping, since it could be extremely interesting.

As we have mentioned in Chapter 2, radiation from coherently-emitting, compact sources becomes important at long wavelengths. Such radiation is often circularly polarized. Interaction of long wavelength radiation with astrophysical plasmas can also result in differential absorption of one of the circular modes, and resultant circular polarization. It therefore seems imperative that we should require a dual circular polarization capability.

5.1.4 U-V Coverage

We have previously noted that the noise level produced by a correlator at these frequencies is totally dominated by the background sky, not by the receiver noise. This situation means that maps made at these frequencies can greatly suffer from the effects of incomplete u-v coverage. There are two distinct, but related, effects. The first is the well-known phenomenon of aliasing, in which emission actually lying outside the map plane appears inside. Aliasing is caused by the use of fast Fourier transforms, and it appears unreasonable to expect use of any other algorithm. Use of good convolution algorithms can reduce aliasing considerably, but the effectiveness of these algorithms depends on the completeness of the u-v coverage. The second effect is the presence of sidelobes in the map from sources lying outside of it. This is a fundmental effect which is independent of the method of transformation. The only solution is to lower the sidelobe levels of the synthesized beam, which means filling the aperture plane as densely as possible.

The current placement of antennas in the VLA leaves considerable empty regions in the outer parts of the u-v plane. This is not a problem when observing in a high-frequency environment where the noise is dominated by the receivers, but it is an undesirable situation for the proposed array. We recognize two ways of correcting this coverage problem:

1) More antennas. An approximately linear filling of antennas along the arms of the current array would give superior filling of the u-v plane.

2) Bandwidth synthesis. Here, observing is carried out at two or more frequencies separated by ~10%.

The superior solution is to add more antennas and locate them in places chosen to optimize coverage. However, as the antenna costs are likely to

dominate the total cost, this solution may be unfeasable. Thus, we initially choose to adopt bandwidth synthesis as the preferred method of increasing u-v coverage, but note that adding more antennas in the future is desirable. The array design should allow both wide frequency coverage and inclusion of more than one bank per current VLA antenna.

It is of the greatest advantage to increase the resolution beyond the ~25" given by the 35 km aperture at 75 MHz. To do this means placement of antennas at distances of 70 km or more. With the advent of the VLBA, sites chosen for their optimal connection to the VLA are being considered. We feel that it is very important to add low-frequency capability to these sites. In particular, the Pietown site will double the resolution of the 75 MHz array for northern declinations. Use of the Los Alamos site would provide angular resolution of better than 10 arcseconds.

5.2 Design Parameters

5.2.1 Antenna Design

5.2.1.1 Primary Element

By primary element we mean the basic antenna used for the array. We cannot use the 25m antennas for two reasons. Firstly, (and most importantly), use of these antennas would violate our first design constraint - not to interfere with the currently existing array. Secondly, their use would require a feed design similar to the 327 MHz system but scaled up to the wavelength of ~4 meters. This requires a feed of about 3.6 meters diameter. If mounted to the side of the subreflector, the resulting beam offset would be about 20 degrees, with unacceptable beam ellipticity and coma sidelobe. To avoid these problems, either the subreflector would have to be removed (one man-day per antenna), or the low frequency feed would have to be mounted directly under the subreflector, blocking it entirely. These solutions are not acceptable.

The remaining choice is to construct new antennas near the existing stations. These could comprise groups of low frequency antennas phased together to form a basic unit. These groups, called banks, will be discussed in chapter 5.2.1.2. The antenna elements should have the following characteristics:

1) They must be small enough to be steerable, either individually or in groups.

2) They should have good forward gain and back-to-front ratio. The latter requirement is necessary to prevent ground reflections from interfering with the primary response.

3) They must have approximate circular power patterns with the inner few degrees being the most important.

4) They should have low cost and ease of construction in view of the large number required.

The simplest antenna is the common, commercially-available Yagi. Since it is linearly polarized, two elements at right angles are needed for circular polarization. Its major drawback is that it has narrow bandwidth - normally about 6% of the operating frequency. This is barely adequate to obtain the bandwidths we desire, and would preclude adjusting frequencies easily to react to changing interference environments. The narrow bandwidth of the Yagi can be circumvented if we utilise log-periodic antennas - these are somewhat similar in construction to the Yagi, but have lower forward gain. A practical solution could be to use log-periodic antennas designed to have broad radiating regions and relatively narrow bandwidth; 60 to 90 MHz - for example. The gain of such an element should approach that of a Yagi.

Another option may be to use helical elements. These have a number of significant advantages - they are naturally circularly polarized, have high

forward gain (depending on the number of turns), and have an enormous bandwidth, about twice the central frequency. This means that if we construct helical antennas centered at 75 MHz, we will be able to cover the entire range from 60 MHz to 180 MHz, enabling multi-frequency operation with its significant advantages. The main drawback seen at this time to helical antennas is that they are more difficult to build and support than the Yagi or log-periodic antennas and, for dual circular polarization, counter-wound helices would be needed. They are not easily available commericially.

Further study may show that the simplest way to obtain the required collecting area is with some type of reflector element, i.e. crude, flimsy dishes somewhat similar to the Culgoora antennas. One of the principal advantages of this choice is that the active element could be made quite simply.

5.2.1.2 Bank Design

In Chapter 4 we argued that calibration of the array can be acheived by using the stronger sources within the target field, and in Appendix A have shown that the required bank directivity is approximately

$$D = 2SNR/(\theta\lambda^{1/2})$$

where λ is the observing wavelength in meters, θ is the observing field of view in radians, and SNR is the signal-to-noise on a baseline necessary for calibration. Our view is that the minimum SNR must be ~1. At 75 MHz, with a one degree field of view, the minimum required gain is ~18db. A much safer level for calibration is with SNR = 3, for which the gain is ~23db.

This rather high forward gain can be achieved with some types of single antennas. For helical antennas, 18dB gain will be attained with a 23 turn antenna of pitch angle 12.5° and 1λ circumference. This means a length of 5λ, or 20 meters at 75 MHz. This is rather long, and it is probably more

practical to use a bank of four smaller elements phased together. In this case, each element needs a forward gain of 12dB, which can be supplied by a 5-turn helical antenna. The corresponding length is 1.2λ or 5 meters. The array will have to be mounted on a flat ground plane of 2.5 wavelengths (10 meters) on a side. Since the frequency is low, the ground plane need not be solid.

A single Yagi or log-periodic element cannot achieve 18dB gain, so if this is the chosen element, a bank of at least four must be used.

The bank must be fully steerable, and preferably equatorially mounted, so that confusing sources in sidelobes are observed with constant amplitude. The drive mechanism need not be especially rugged as we do not envisage rapid motion of the bank. If the banks are equatorially mounted, the right ascension drive is the only one which needs to track continuously.

It is clearly desirable to have a bank beam which minimizes levels. At 75 MHz, the required physical size of the ground plane will restrict the number of elements to no more than 4 or 5 so that little opportunity to shape the combined response exists. At a higher frequency, the number of elements could be increased to 9 or even 16 while still maintaining the same physical size. This would allow feeding the component elements with different weightings and so obtain a much improved beamshape.

An alternative design would have the component elements on their own mounts. This is an inferior alternative as each would have to be phased individually. Furthermore, the changing separation as the source is tracked will modulate the primary response due to changing mutual impedences as well as the usual foreshortening effects.

Assuming that this proposal receives wide support and is implemented, our next task will be to seriously attack the question of the antenna

element and bank design. Our requirements can be stated simply; we need to obtain ~100 to 200 m^2 of equatorially mounted, reasonably wide-band, dual-circular polarization collecting area at the lowest possible cost.

5.2.2 Pre-Amplifiers

The calculations of signal-to-noise ratios given in chapter 4 assumes no other source of noise except the background sky. A possible significant noise source is cable losses between the banks and the amplifiers. To prevent significant deterioration of the signal, we require a relatively low-noise amplifier located with each bank. Good wide-band, low noise amplifiers are now available off-the-shelf, so the acquisition of these amplifiers should not be a problem. It is essential to use amplifiers with good intermodulation characteristics since some of the low-frequency interference is extremely strong. The signals must be conducted to the nearest antenna via a buried coaxial cable. To prevent gopher interference, the cable should be encased. Also important are good filters to reject out-of-band interference.

5.2.3 Signal Transport

The cheapest way by far to transport the signals is through the current waveguide system. There appear to be two ways to do this. The first is to make use of one of the spare waveguide channels. This would allow the low-frequency array to run at all times, independent of the positions of the 25-m antennas. However, this is also an expensive option, as new waveguide couplers and an independently operating electronics system would need to be constructed. A much cheaper option is to use the current antennas, and piggy-back the signals upon the waveguide channel used by that antenna. The disadvantage of this technique is that the low-frequency array will only

operate when antennas physically occupy the 'A' array stations - approximately 1/4 of the total time. We do not regard this to be a severe liability at the present time, as enough data can be taken in this interval to keep the post-processing system busy. Furthermore, in view of the vastly increased cost (a factor to 2 to 3) needed to provide full-time observing, it seems wise to adopt the minimum approach.

The simplest arrangement would be to conduct the amplified signals to the nearest antenna where the signal will be mixed to a convenient frequency for transport via the waveguide to the correlator. Each waveguide channel contains approximately 2 GHz bandwidth, and less than half of that is currently occupied. There appears to be plenty of room for narrow bandwidth signals. The total bandwidth of this array is less than 10 MHz - representing only 4% of the current waveguide power levels. Each antenna contains 1200 and 1800 MHz local oscillator signals, and one possibility is to use these to convert the low frequency signals to intermediate frequencies ready for transport through the wave-guide system.

It does not seem feasible to consider transporting the entire useable bandwidth provided by the banks, since this will both considerably increase the power in the waveguide, and will contain large and time-variable interference. Presuming the final 4 MHz bandwidths only will be inserted to the waveguide, the frequency and bandwidth selection must be done at the antennas. This will be done by first up-converting to an IF in the 200 to 300 MHz range with a variable frequency local oscillator. All images are thus placed well outside the antenna and preamplified bandpass. Fixed frequency local oscillators will convert the signals to the frequency appropriate for insertion into the currently operating electronics. The first local oscillator frequency will thus determine the observing frequency.

The point for inclusion of the low-frequency signals into the VLA system occurs well after the existing Walsh function generator. It is important to prevent offsets causing correlation errors, so the Walsh function switching must be applied to the low- frequency signals. If more than one bank is to be passed through one antenna, both can use the same Walsh functions, and their products will be ignored by the correlator.

An attractive alternative is to digitize the signals at the antenna and transport the bit stream through the waveguide system. A digital system should be immune to correlator offsets, thus removing the need for applying the Walsh functions. Since the bandwidths are relatively narrow, this process may be practical.

Upon receipt of the signals at the control building, final amplification, bandpass shaping, and frequency conversion would be done, and the signals would be ready for recording or, after insertion of phase shifts and delays, correlation.

5.2.5 Control System

Since the current VLA on-line (Modcomp) computer system will soon be upgraded to a system with considerably greater capacity, and since any separate computer running the low frequency array would have to communicate through the Modcomps, it is preferable that the new Modcomps handle the low-frequency array as well as the current VLA. The load increase due to the low-frequency system is very small and this extra load should be easily handled.

A limited amount of control information must be passed to the individual banks. This would include the tracking and slewing information. There is sufficient spare capacity built into the current system to handle the load. If frequency and bandwidth selection are required at the antenna

(as is likely), this must also be done using the spare capacity. ALC levels must be returned from the antennas.

The low frequency array will not require complex control. It is a vastly simpler system than the current VLA, and the only contemplated mode of observing uses long sessions. The electronics will require little on-line monitoring.

Current plans for upgrading the Modcomps include the impact of this system.

5.2.6 Data Recording

The advent of wide-bandwidth recording systems, notably the Mark III VLBI system, allows an extremely flexible observation mode for the proposed array. In this mode, the data are recorded on tape rather than directly correlated. The advantages of this approach are considerable. The greatest one is that the entire field seen by the bank can be synthesized by repeated passes of the recorded data through the correlator, adjusting the phase and delay tracking on each pass. Thus, when the observing conditions are good, maximum use of the data can be made. Furthermore, a quick check of data quality can be performed by phasing to the strongest source in the primary beam on the first pass. If the phase behaviour is poor, the entire run can be purged, and new data taken. In this way, only good data will be saved.

This mode also will greatly reduce the computer load. Since data will be kept from good observing days only, the isoplanatic patch sizes will be large, allowing larger maps (hence, fewer maps), and far simpler self-calibration. Only the brightest sources will be needed for the model.

5.2.7 Correlator

Because we strongly advocate near-complete independence of this system from the current VLA, we believe that a separate, dedicated correlator

should be built. There is no justification for removing half the correlator capability of the current system for a continuum system of less than 4 MHz bandwidth, especially since the cost of a new, dedicated correlator is low.

The simplest correlator is a single frequency, 27-antenna system which correlates a single polarization only. However, we have argued in 5.1.3 that polarization capability is important. Including all four polarization correlations, the resulting correlator is 0.01 of the current VLA correlator, and could probably be built for less than $50K.

We have argued in Sec 5.3 that it is desirable to use more than 27 stations in order to obtain better u-v coverage. Taking, for simplicity, 54 stations we will require a correlator 4 times larger than the one mentioned in the previous paragraph, making it equal to .04 VLA correlator units. Ray Escoffier's estimate for such a correlator is $50K to $75K. The use of so many elements may be precluded by cost, but an expansion to this size should be kept in mind. It appears that a dedicated correlator sufficient for this array can be constructed for $50-100K. Although superior for numerous reasons, a spectral-line correlator greatly escalates the total cost, and is not justified at this time. As a temporary measure, the current VLA correlator is probably idle enough of the time to allow initial testing of the low-frequency system.

5.3 Data Processing

We expect that regular calibration of the data is unnecessary, so there seems to be no need to utilize the Dec-10 in the data flow. We believe that the data should be written straight onto tape following correlation. The data rate will be set by the timescale over which antenna phases change by a significant fraction of a radian, or by the time in which visibilities of sources within the useful field of view change by a significant fraction of

a radian, whichever is shorter. This timescale is likely to be at least 1 minute, and perhaps as long as three, depending on the field of view. These slow data rates imply modest database sizes.

The data will be calibrated on the post-processing system, which we will assume to be a VAX (although any other comparable machine will do). A model of the target region will be supplied, and calibration attempted. It is difficult to anticipate the amount of computer power required for this operation, since it depends on many ill-defined or incompletely known factors. In particular, the field of view and the gain change time-scale are particularly important. We have argued in Chapter 4 that the field of view can be limited to ~1 degree by combining bandwidth and time-averaging effects. The viability of this will have to be tested. In setting limits for an acceptable time- scale, we must have some idea of the distribution of time-scales. If 10-min timescales are common, then we will have no qualms about throwing away data with 5-minute timescale, and the calibration problem is simple. If however, the typical timescales are less than a minute, than calibration becomes very much more difficult and will require greatly increased computer power. In fact, we have little to no idea of the typical time-scales although, on the basis of arguments presented in Chapter 3, we expect minutes. The only real way to answer this important question is to take test data, and we expect to use the 327 MHz system to help us in this.

Assuming that the antennas are in operation about 25% of the time, and presuming that we shall keep data whose time-scales are greater than about 1 minute, (which may be about 50% of the total data), we do not anticipate a heavy computer load. An extremely rough estimate is 1/2VAX, including an array processor. We shall only discover the real impact after enough data

is taken to set the usuable and usual time-scales, interference environment, isoplanatic patch size, corresponding map size, and number of iterations required for calibration to converge.

6. COST, TIME, AND MANPOWER REQUIREMENTS

The current RE budget of the VLA is heavily committed through 1985. In 1984-1985 the major items are the 330 MHz system, water vapor radiometers, the synchronous computer upgrade, and various items for data processing and storage. These items cannot be displaced or deferred. In 1986 it may be possible to commit significant resources to the 75 MHz project.

Assuming that this proposal recieves sufficient support from the user community that a decision is made for it to proceed, we would propose the following tentative schedule:

June - Sept 1984.

Study and finalize the antenna element and bank design. Monitor RFI spectrum.

October - December 1984.

Study ionospheric stability using long VLA baselines at 327 MHz. Monitor RFI spectrum.

Summer 1985.

Build prototype antennas and a simple interferometer at 75 MHz.

Winter 1985.

Test prototype interferometer. Set up contractual arrangements for antenna construction and installation.

Spring - Summer 1986.

Antenna construction. Detailed design of electronics and data recording system.

Fall - Winter 1986.

Electronics construction. Initial data recording and testing. Software development.

1987.

Initial operation of 27 element system. Software devlopment and testing. Completetion of system at the VLA site. Construction of antennas at nearby VLBA sites and integration with VLBA system.

Cost Estimate

1984	Paper studies of antenna design	
	RFI Monitoring	$10K
	327 MHz tests	
1985	Prototype interferometer and tests	$20K
1986	27 antennas at $10K each	$270K
	28 sets of electronics to be installed in 25-meter antennas at $8K each	$224K
1987	Dual-channel correlator (incl. back-end electronics)	$100K
	VLBA tape recording system	$66K
	Subtotal	$690K
1988	VAX-type computer (one-half)	$300K
	Antennas at VLBA sites	$100K
	Grand Total	$1090K

The manpower requirements are modest. We roughly estimate that ~5 technical man-years' labor will be required.

Fig 1 RFI from 68 to 88 MHz

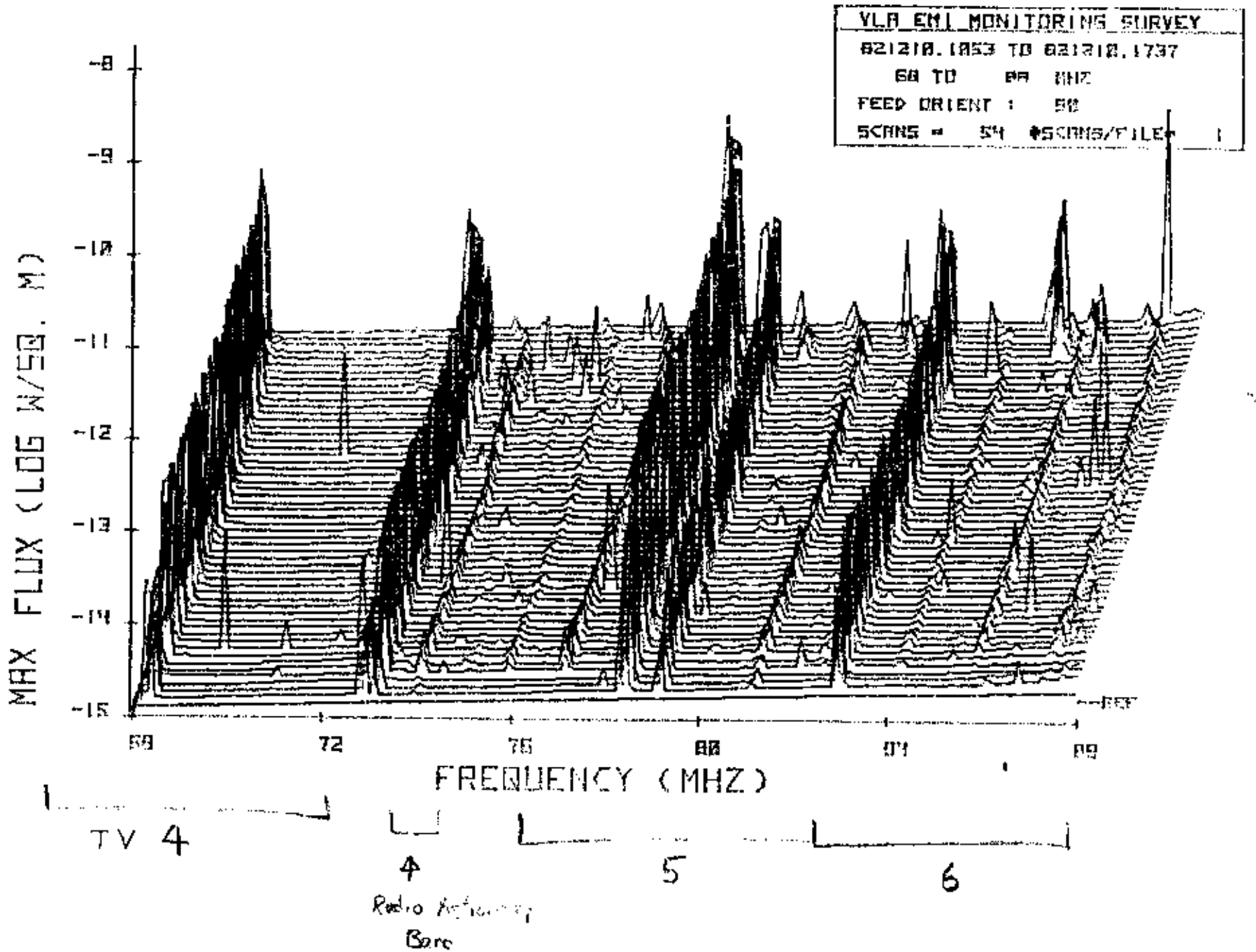

Fig 2. RFI from 100 to 150 MHz.

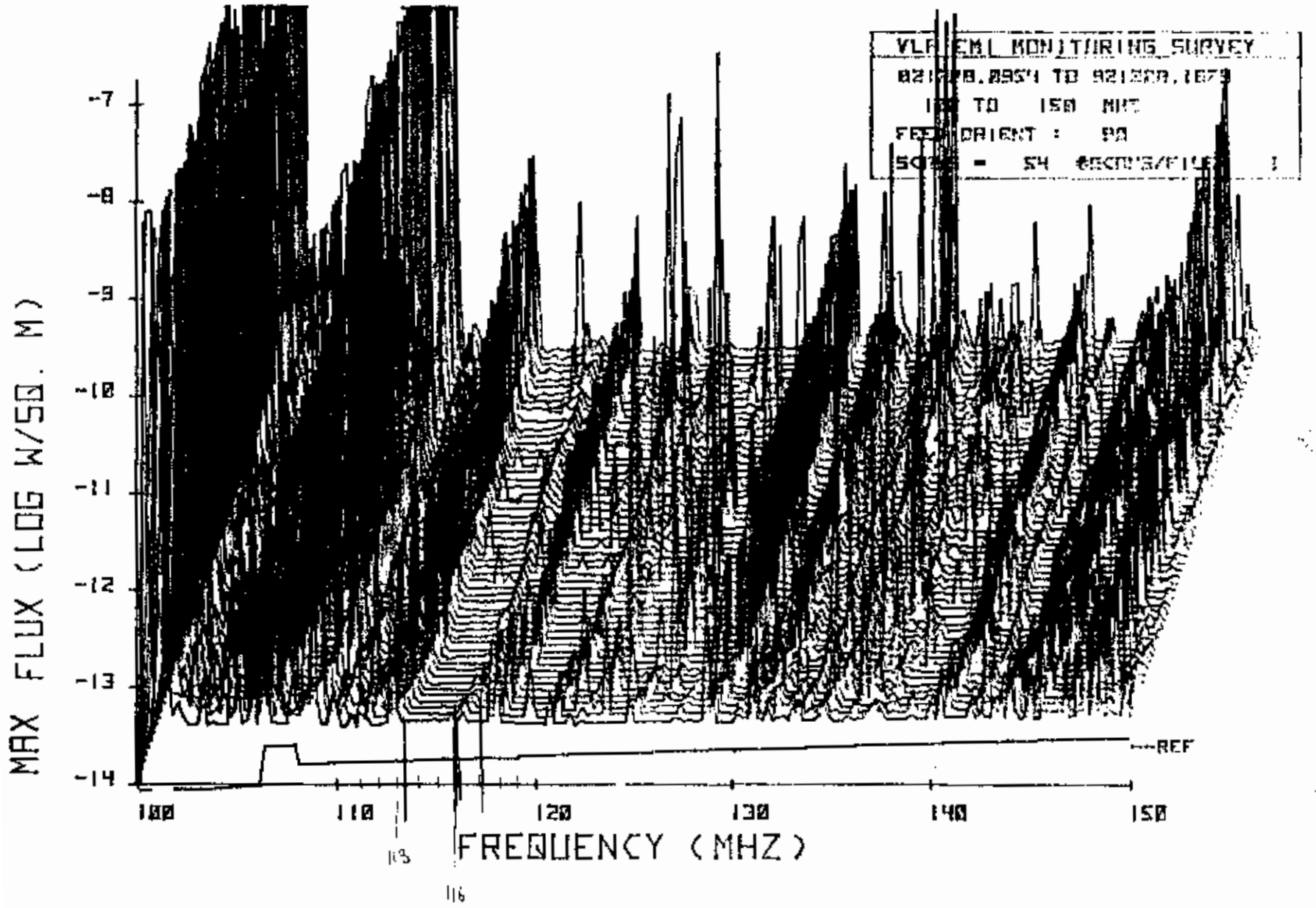

Fig 3. RFI from 150 to 200 MHz

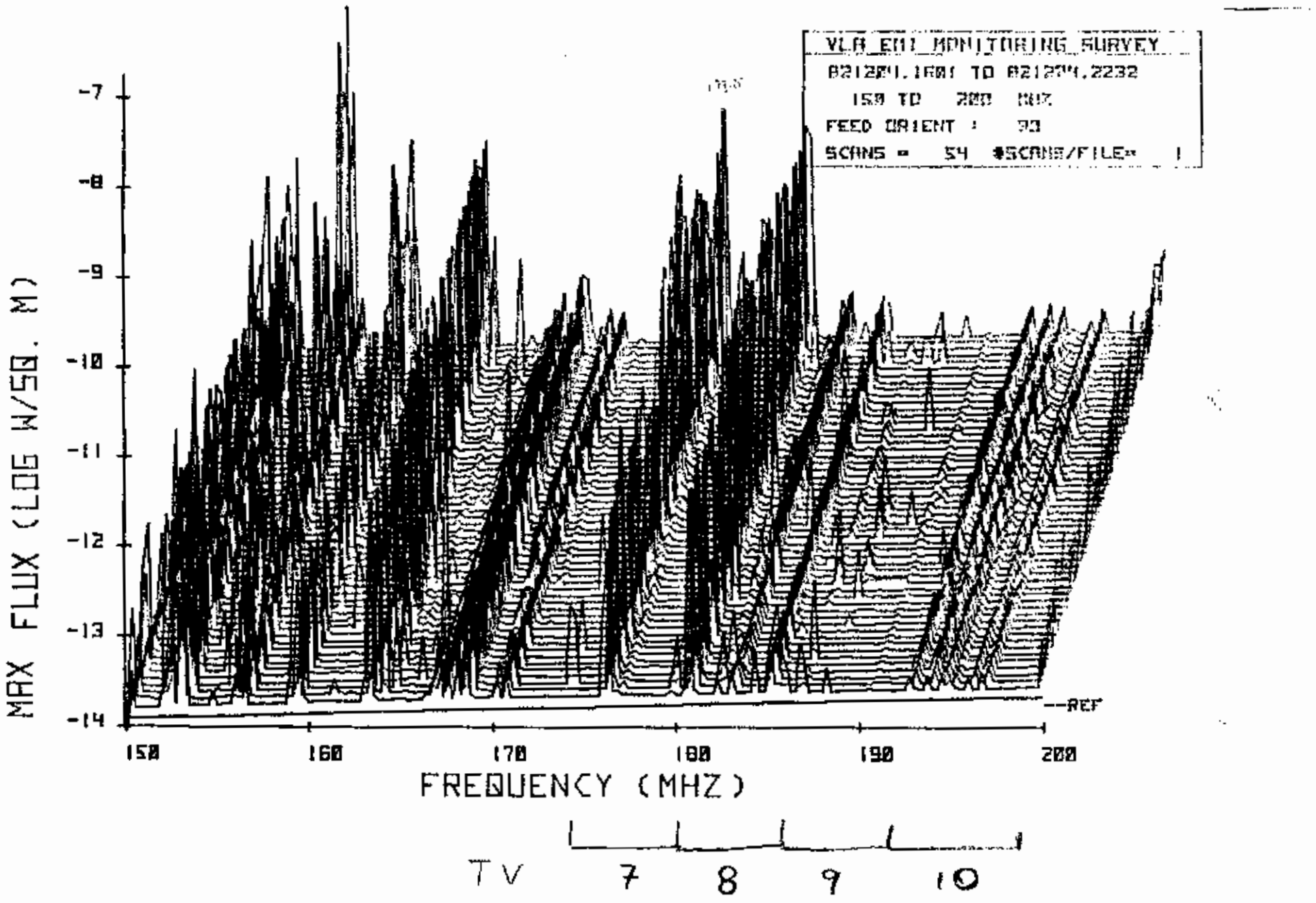

APPENDIX A.

SIGNAL AND NOISE IN LOW-FREQUENCY RADIO INTERFEROMETRY

In this appendix we describe in detail the calculations required to estimate the noise which arises in low-frequency observations with an interferometer. The noise has two origins, the familiar fluctuations due to receiver and sky noise, and fluctuations due to passage of background sources through the interferometer fringe pattern. We describe these two sources separately.

A-1. Thermal Noise

We have shown in Chapter 4 that the total system temperature of a low-frequency radio telescope is dominated by the (galactic) sky background. Under this condition, Napier and Crane (Chapter 3 of the Synthesis Mapping Workshop) show that the expression for the rms output fluctuations becomes:

$$\sigma = S_T/(2Bt)^{1/2}.$$

Here, S_T is the total flux density seen by the antenna, t and B are the integration time and bandwidth respectively. Assuming a smooth background emission, the total flux density seen by the antenna is:

$$S_T = 2kT_{sky}/A_e,$$

where A_e is the effective antenna area. The sky temperature away from the galactic plane can be approximated by $T_{sky} = 20F^{2+\alpha}$, where F, the normalized frequency parameter is $408/\nu_M$, with ν_M the frequency in MHz. Combining these equations, the rms noise in Janskys is found to be:

$$\sigma_t = 40F^{2+\alpha}A_e^{-1}(B_M t)^{-1/2}.$$

This assumes a perfect analog correlator. In practice, a digital correlator will almost certainly be used. If we assume a three-level system like the current VLA correlator, the noise estimate must be raised by approximately 20%. We thus estimate the rms noise on a single correlator to be:

$$\sigma_t = 50F^{2+\alpha}A_e^{-1}(B_M t)^{-1/2}.$$

In terms of the antenna main beam solid angle, Ω_M, the noise is:

$$\sigma_t = 90F^{\alpha}\Omega_M(B_M t)^{-1/2}.$$

At 75 MHz with 1 minute averaging and 100 m^2 bank area, the rms noise is approximately 6.6 Jy.

These expressions describe the output fluctuations due to a smooth uncorrelated background source. The fact that the system temperature is dominated by the background sky indicates that the influence of discrete sources may be important in the determination of system parameters. There are two effects to consider: 1) The summed flux density from the sources within the antenna beam will contribute to the system temperature, and 2) The passage of these sources through the interferometer fringe pattern will create an effective noise which may be larger than the thermal noise. Evaluation of both these quantities requires knowledge of the background differential source count, n(S).

A.2 The Differential Number Count

We have used the normalised, differential number count given by Pearson (MNRAS 171, 475 (1975)), taken from the 408 MHz 5C counts, the Molongo MC1 survey, and the whole-sky source compilation. The count, shown in Fig. A-1, is normalized by an Euclidean number count of 750 sources/steradian above 1 Jy at 408 MHz.

For conversion to a simple analytic form, we have broken the count into three regions, with boundaries at 0.8 Jy and 10 Jy. These regions are denoted I, II, and III, in order of decreasing flux density. The power law indices are (with respect to the Euclidean count), -0.7 in region I, 0.0 in region II, and 0.7 in region III. The approximations are excellent in

regions II and III, but there are significant deviations in region 1. This error is of significance only when evaluating the second moment. To convert the 408 MHz count for use at any frequency, we assume that all sources have the same spectral index, α. This should be an excellent approximation for frequencies lower than 408 MHz, as there are few flat spectrum sources with appreciable flux density in this range, and the dispersion in the spectral index amongst steep-spectrum objects is small.

The resulting differential number count, n(S), is:

Region I: $n(S) = 7600F^{2.2\alpha}S^{-3.2}$ $\quad 10F^{\alpha}<S<50F^{\alpha}$

Region II: $n(S) = 1500F^{1.5\alpha}S^{-2.5}$ $\quad 0.8F^{\alpha}<S<10F^{\alpha}$

Region III: $n(S) = 1750F^{0.8\alpha}S^{-1.8}$ $\quad .001F^{\alpha}<S<.8F^{\alpha}$

where S is the flux density in Jy at the desired frequency, and $F = 408/\nu_M$ with ν_M being the frequency in MHz.

We have selected a flux density of $50F^{\alpha}$ as the upper limit to the number count as the few sources above this level will not affect the results in any important way. There are only 16 such sources in the 3C catalogue; almost all are of sufficient size that they will be resolved out to the baselines of the proposed array.

The 5C counts are valid only to .01 Jy at 408 MHz, but the lower limit of .001Jy has been selected since recent number count experiments done at 1400 MHz with the VLA indicate that this extrapolation is valid. This extension has little effect on any important result.

The approximations given above are shown superposed on the number count in Fig. A-1.

A.2.1 Zeroth Moment (Integral Number Count)

The integral number count is found by integrating the differential count over the relevant range. We calculate the quantity <N> = the mean

number of sources/steradian with flux density greater than S. Within the three ranges given above, the results are:

I. $\langle N \rangle = 3450F^{2.2\alpha}S^{-2.2} - 0.63$

II. $\langle N \rangle = 1010F^{1.5\alpha}S^{-1.5} - 10$

III. $\langle N \rangle = 2200F^{0.8\alpha}S^{-0.8} - 1230$

The total number of sources/steradian within the three ranges are 21.5, 1400, and 5.53×10^5, respectively. The total number of sources per steradian over the given number count is 5.54×10^5.

A.2.2 First Moment (Total Flux Density per Steradian)

The mean flux density per steradian in sources above flux density S is given by $\langle S \rangle = \int Sn(S)dS$ integrated over the range from S to $50F^{\alpha}$. The results are given below in the three ranges.

I. $\langle S \rangle = 6330F^{2.2\alpha}S^{-1.2} - 58F^{\alpha}$

II. $\langle S \rangle = 3030F^{1.5\alpha}S^{-0.5} - 620F^{\alpha}$

III. $\langle S \rangle = 11220F^{\alpha} - 8830F^{0.8\alpha}S^{0.2}$.

At the range boundaries, there are $340F^{\alpha}$ Jy/ster above $10F^{\alpha}$, $2780F^{\alpha}$ Jy/ster above $0.8F^{\alpha}$ Jy, and $9000F^{\alpha}$ Jy/ster to the bottom of the known number counts. Although only .004% of all sources lie in region I, they contribute 3.7% of the total flux density. Similarly, the 0.25% of all sources residing in region II contribute 31% of the total flux density. At 75 MHz, we find there is 9.8 Jy per square degree.

A.2.3 Second Moment (Mean Square Flux Density)

The mean square flux density $\langle S^2 \rangle$ due to sources with flux density greater than S is given by $\int S^2 n(S)dS$ integrated over the range S to $50F^{\alpha}$. The results are given below in the three ranges.

I. $\langle S^2 \rangle = 2.65 \times 10^4 F^{2.2\alpha}S^{-0.2} - 1.30 \times 10^4 F^{2\alpha}$

II. $\langle S^2 \rangle = 1.62\times10^4 F^{2\alpha} - 3040F^{1.5\alpha}S^{0.5}$

III. $\langle S^2 \rangle = 1.47\times10^4 F^{2\alpha} - 1470F^{0.8\alpha}S^{1.2}$

The results of this calculation are strongly dependent upon the upper limit. The result of increasing this limit of integration to $100F^{\alpha}$ would be to add $2220F^{2\alpha}$ to each range above. We believe that due to the size of these few sources, their contribution can be neglected.

The total mean square flux density is $1.47\times10^4 F^{2\alpha}$ $(Jy/ster)^2$ so the r.m.s. level is $121F^{\alpha}$ Jy/ster. Most of this originates from regions I and II.

A.3 Background Source Contribution to System Temperature

The total flux density in background sources within a beam pattern $B(\ell,m)$ is $S_T = \int Sn(S)dS \int Bd\Omega$. Using the preceding calculations, the integration gives $S_T = 9000F^{\alpha}\Omega_B$ Jy, where Ω_B is the all sky integral of the antenna beam. This flux density corresponds to an antenna temperature of $T_{bs} = 1.8F^{2+\alpha}$ K. Thus, the contribution to the total system temperature by discrete sources is less than 10% of the background continuum contribution and can be ignored.

A.4 Confusion Signal

We have outlined in Chapter 3 our proposed method of calibration. This is to utilize the strongest background sources in the undistorted field of view as calibrators and, using selfcalibration techniques, determine the antenna gains. To enable calculation of the signal and noise available to this technique, we must put the number count and its moments into more useful form.

The total flux density from background sources in a solid angle Ω is easily found from integrating the number count to be $9000F^{\alpha}\Omega$. A valuable

function is the number of sources/steradian, counting down, which contribute a fraction f of the total available flux density. This function can be found to be:

$$\text{Region I:} \quad N(f) = 6570(f + .0064)^{11/6} - 0.63 \qquad f<.037$$

$$\text{Region II:} \quad N(f) = 26400(f + .069)^{3} - 10 \qquad .037<f<0.31$$

$$\text{Region III:} \quad N(f) = 2040(1.247 - f)^{-4} \qquad f>0.31$$

The three regions correspond to the three different power law approximations to the differential number count.

The flux density S_f at which this fraction is obtained is easily found to be:

$$S(f) = 0.746F^{\alpha}(f + .0064)^{-5/6} \qquad f<.037$$

$$S(f) = 0.1153F^{\alpha}(f + .069)^{-2} \qquad .037<f<0.31$$

$$S(f) = 1.1F^{\alpha}(1.247 - f)^{5} \qquad f>0.31$$

The Table in Chapter 4 is taken from these expressions.

A.5 Confusion Noise

Providing that an interferometer baseline is very much larger than the antenna size, the effect of background sources on the interferometer output can be viewed as a two-dimensional random walk problem. The analysis is presented in Appendix B, where it is shown that the mean square fluctuations about the mean are given by:

$$\sigma_c^{\,2} = 0.5[\int S^2 n(S)dS][\int B^2 d\Omega]$$

where B is the antenna power pattern. To evaluate this contribution, we require the second moment of the number count and the squared beam integral.

A.5.1 Evaluation of the Second Moment

Evaluation of the second moment of the number count is complicated by the necessity of selecting reasonable limits to the integrations. The choice of an integration range is made on what one considers as signal and

what is noise. Our suggested calibration procedure uses as signal the flux density from background (and target) sources within the smallest isoplanatic, undistorted region. We thus adopt the following practical definition: we use as signal the N sources of highest flux density (representing a fraction f of the total flux density) within the available solid angle Ω. This angle will generally be set by the combination of bandwidth and time-averaging effects, and as we discuss later, should be less or equal to the isoplanatic field of view. The confusion noise is then evaluated from the unmodeled sources lying within Ω plus a contribution from all sources lying outside this area. For this integration, we have chosen an upper flux density limit of $50F^{\alpha}$ as discussed in Sec. A.2 and A.2.3. The resulting second moment up to this limit is $1.47\times10^{4}F^{2\alpha}$.

Evaluation of the noise from sources below flux density $\dot{S}(f)$ requires integration over a different range than given in A.2.3. When integrated only up to that flux density level above which a fraction f of the total flux density is obtained, the second moment becomes:

$$\text{I.} \quad 32000F^{2\alpha}[1 - 1.26(f + .0064)^{1/6}] \qquad f<.037$$

$$\text{II.} \quad 1010F^{2\alpha}[(f + .069)^{-1} - 1.55] \qquad .037<f<.31$$

$$\text{III.} \quad 1637F^{2\alpha}[(1.247-f)^{6} - 2\times10^{-4}] \qquad f>.31$$

It appears that a reasonable goal is to model half the flux density in the modeling region, as this requires prior knowledge of the flux densities and positions of only the strongest 1.2% of the integral number count, corresponding to a source density of ~2 per square degree. For f between 0.31 and ~0.8, the second moment from sources below the corresponding flux density level can be well approximated by:

$$\langle S^{2}\rangle = 1637F^{2\alpha}(1.247-f)^{6}.$$

The confusion level can then be expressed as

$$\sigma_c^2 = F^{2\alpha}[7350\int_s B^2 d\Omega + 820(1.247-f)^6 \int_m B^2 d\Omega].$$

The subscript 's' under the first integral sign signifies integration over the unmodeled solid angle, while 'm' indicates integration over the modeled region. From this expression it is clear that the noise from sources lying outside the modeling region will dominate the total confusion noise unless the antenna beam shape and the effects of bandwidth and time-averaging can reduce this contribution to less than a few percent of the noise from unmodeled sources within the modeling region.

A.5.2 Evaluation of the Beam Integral

It remains now to calculate the integral of the squared beam response for the field of view, and outside it. We emphasize here that the beam is that appropriate to a baseline, and is not the synthesized beam of the array.

It is clearly undesirable for the field of view set by the combination of bandwidth and time averaging to be larger than the isoplanatic size, for in this case, sources which cannot be modeled will contribute to the confusion noise. We therefore must have the mapping field of view equal to or smaller than the isoplanatic field of view. The mapping field of view is set by bandwidth and time averaging, as the influence of the bank beam is minor unless it is of comparable angular extent, a condition unlikely to be met in practice. At the north pole, the effects of bandwidth and time averaging are equivalent and orthogonal. At other declinations the situation is more complicated, but we will nevertheless presume the effects remain orthogonal in order to obtain simple expressions for the beam integrals. The procedure is then to obtain functional relationships for the two effects and multiply them to obtain the effective beam.

In order to compare the contributions to the total noise from thermal and confusion effects, we will assume a worst case for confusion suppression - a square bandpass, and simple boxcar time averaging. We define the main beam to be that region lying within the first zero crossings of the resultant sky pattern. In this case, we show in Appendix C that the squared integrals for the main beam and sidelobes are:

$$\int_m B^2 d\Omega = 2.5/(\nu_M B_M t),$$
$$\int_s B^2 d\Omega = 0.56/(\nu_M B_M t).$$

In these calculations, a baseline of 20 km has been chosen, since this represents the 'typical' baseline we intend to use for calibration. Clearly, the shorter baselines will contain considerably more confusion, and it will probably prove necessary to ignore data taken on shorter than ~10 km baselines for the calibration process. Inserting these values, we find, for the confusion noise:

$$\sigma_c = 45F^{\alpha}(\nu_M B_M t)^{-1/2}[2+(1.247-f)^6]^{1/2}.$$

The confusion noise is dominated by the contribution from the sidelobes, and is only weakly depending upon the fraction of the total flux density being modeled. For f = 0.5, a reasonable value, the confusion noise becomes

$$\sigma_c = 65F^{\alpha}(\nu_M B_M t)^{-1/2}.$$

The ratio of thermal to confusion noise can now be calculated to be:

$$\sigma_t/\sigma_c = .75F^2\nu_M^{0.5}/A_e.$$

At 75 MHz, this ratio becomes $192/A_e$, and indicates that the thermal noise due to the galactic background will dominate providing bank areas are less than ~200 m^2, as is most likely. Improving the filter shape to reject confusion will make this ratio larger.

4.4 Signal/Noise Ratios

Within the undistorted field, the flux density available for calibration is $9000fF^{\alpha}\Omega$. Presuming the field of view is set by the bandwith and time-averaging, the integral over the main beam is $4.24/(\nu_M B_M t)$, a result which is not strongly dependent upon the detailed bandpass shape. As the thermal noise dominates, the resulting signal-to-noise ratio becomes

$$SNR = 100f(B_M t)^{1/2}\Omega_{mod}/\Omega_{MB}.$$

In this expression, Ω_{mod} is the solid angle of the modelled area, Ω_{MB} is the bank beam solid angle. This expression can be cast into different forms:

$$SNR = 8fD\Omega_{mod}(B_M t)^{1/2},$$

where D is the bank directivity, and

$$SNR = 1.1\times10^{-3} f A_e \nu_M^{\ 2} \Omega_{mod}(B_M t)^{1/2}.$$

where A_e is the bank effective collecting area. By matching the bandwidth and time averaging field of view to the isoplanatic size, and presuming square filters and boxcar time averaging, the following forms can be derived:

$$SNR = 1/1D\Omega_{mod}^{\ 1/2}\nu_M^{\ -1/2},$$

$$SNR = fD\theta_{iso}\lambda^{1/2},$$

and

$$SNR = f\nu_M^{\ 3/2}\theta_{iso}A_e/400.$$

Chapter 4 draws from these expressions.

APPENDIX B

THE CALCULATION OF CONFUSION NOISE

This appendix calculates the rms noise in a complex correlator due to the passage of a large number of background sources through the interferometer fringe pattern. We assume that the interferometer consists of two identical banks, each with an element beam $B(\ell,m)$, which are connected with a perfect complex correlator. The response of the interferometer to a source of spectral flux density S is then $\underline{s}_i = SB(\ell,m)\exp(i\theta)$, where the phase θ is a function of the baseline length and orientation and of the source displacement from the phase tracking center. In the complex plane, the response can be considered a vector $\underline{s}$ of length $SB(\ell,m)$, and angle θ. The net response over all sources visible to the interferometer at any given time is $R = \Sigma s_i$.

The total number of sources contributing to this sum is very large, and their positions with respect to the interferometer are constantly changing. Further, in the case we are interested in, the baseline length is vastly greater than the element size, which means that the effective field of view contains a large number of fringes, or cycles in phase. Under these conditions, we can consider the net interferometer response to be a random variable, as it is the sum of a very large number of vectors with constantly and differently changing phases and amplitudes. We can regard each contributing response to have a random phase, so that the net response can be treated as a random walk in two dimensions. The average and mean square responses can then be calculated by application of the powerful techniques which have been developed for the random walk process (see, for example, S. Chandrasekhar, Rev. Mod. Phys., 15, 1, (1943), and reprinted in 'Selected Papers on Noise and Random Processes', (1954),N. Wax, ed., Dover Publications).

To find the mean and mean square response, we need to determine $p_N(\underline{R})$, the probability distribution function of R. N here and elsewhere denotes the total number of sources contributing to the sum response. Recognizing the problem as a two-dimensional random walk problem, we must evaluate the integral

$$p_N(\underline{R}) = (2\pi)^{-2}\int \exp(-i\underline{\rho}\cdot\underline{R})A_N(\underline{\rho})d\underline{\rho}$$

where

$$A_N(\underline{\rho}) = [\int p(s_i)\exp(i\underline{\rho}\cdot\underline{s}_i)d\underline{s}_i]^N,$$

and $p(\underline{s}_i)$ is the probability density function for the source of apparent flux density $\underline{s}_i$. We assume azimuthal symmetry (i.e., sources have no preferred phase), so $p(\underline{s}_i) = p(s_i)/(2\pi s_i)$. $p(s_i)$ is the p.d.f. of response s with no regard to angle (phase) for the apparent flux density s_i.

The expression for A_N becomes, after changing to polar coordinates and integrating over the polar angle,

$$A_N(\rho) = [\int p(s_i)J_o(\rho s_i)ds_i]^N,$$

where $J_o(x)$ is the Bessel function of order zero.

To make further progress, we now assume that N, the number of sources is large. In doing so, the Bessel function can then be expanded to second order, so the expression for A_N becomes:

$$\begin{aligned} A_N(\underline{\rho}) &= [\int p(s_i)(1-\rho^2 s_i^2/4 + \ldots)ds_i]^N \\ &= [1-\rho^2\langle s^2\rangle/4 + \ldots]^N, \end{aligned}$$

where $\langle s^2\rangle = \int p(s_i)s_i^2 ds_i$ is the second moment. In the limit of large N, we have

$$A_N(\underline{\rho}) = \exp(-N\rho^2\langle s^2\rangle/4).$$

The p.d.f of the resultant vector $\underline{R}$ is then

$$p_N(\underline{R}) = (\pi N\langle s^2\rangle)^{-1}\exp[-s^2/(N\langle s^2\rangle)].$$

This distribution is Gaussian, with zero mean and dispersion

$$\sigma = [N\langle s^2\rangle/2]^{1/2}.$$

The most probable value of R can easily be shown to be $R = \sigma$.

The dispersion can be related to the differential number count by evaluating the mean square flux density, $\langle s^2\rangle = \int s^2 p(s)ds$. Because the correlator sees not the true flux density S, but rather the flux density $s = BS$ as weighted by the antenna beam, the mean square flux density becomes,

$$\langle s^2\rangle = \iint p(S)S^2B^2 dS d\Omega.$$

The p.d.f is related to the number count by

$$p(S) = n(S)/N$$

so the resulting dispersion becomes

$$\sigma = [\iint S^2B^2 n(S)dSd\Omega/2]^{1/2}.$$

Since the integration over angle is independent of that over the number count (meaning that sources have no prefered place in the sky), we finally get

$$\sigma^2 = [\int S^2 n(S)dS][\int B^2 d\Omega]/2$$

Direct application of Campbell's Theorem (given in 'Mathematical Analysis of Random Noise', S. O. Rice, reprinted in 'Selected Papers on Noise and Stochastic Processes') gives the same result when applied to a cos or sin correlator. Evidently, confusion noise is the same to either a simple or complex correlator.

APPENDIX C

INTEGRATING OVER THE INTERFEROMETER RESPONSE

Realistic integrals over the interferometer response are important in order to calculate the effects of confusion noise, and to judge whether enough signal exists to allow calibration. This appendex shows the methods used to estimate the integrals

$$\int B(\ell,m)d\Omega \qquad \text{and}$$

$$\int B^2(\ell,m)d\Omega.$$

It is convenient to use (ℓ,m) (direction cosine) coordinates as these are the 'natural' coordinates for the interferometer. We orient the coordinates so that ℓ varies in the direction of the baseline vector, i.e. $\ell = \cos(\underline{B}\cdot\underline{s}/|B|)$, where $\underline{B}$ is the baseline vector, and $\underline{s}$ is the unit vector towards the phase center. In these coordinates, the element of solid angle $d\Omega$ is

$$d\Omega = d\ell dm/n$$

where $n = \cos(Z) = (1-\ell^2-m^2)^{1/2}$. The area of integration is the circular plane bounded by $\ell^2+m^2 = 1$. This implicitly assumes we are observing at the zenith, and that there is no radiation from the lower hemisphere.

The beam is considered to be the product of two functions. The first is the bank beam with a typical angular extent of 15 or 20 degrees FWHP. The second function is that describing the bandwidth and time-averaging effects. These are of much smaller size, typically 1 to 5 degrees. We assume the bandpass is square of total width B Hz, and that the time averaging is also rectangular with width t. Then the effects on the sky when observing the north pole are:

a) Bandwidth. $B(\ell) = \sin(C_1\ell)/C_1\ell \qquad C_1 = \pi BL/c$

b) Time. $B(m) = \sin(C_2 m)/C_2 m$ $C_2 = \pi\omega tL/\lambda$

Here, L is the baseline length, λ the wavelength, and ω is the angular rotation rate of the Earth, 7.27×10^{-5} Hz. Although we have made the approximation that observations are made at $\delta = 90^{\circ}$, the resulting expressions should suffice for other declinations.

These functions have their first zeros at $|\ell| = c/BL$, $|m| = \lambda/\omega tL$. Note that both C_1 and C_2 are much larger than one, typically 100 or more, for bandwidths of 1 MHz and averaging times of ~1 minute.

We now approximate the bank beam by cos(Z). This is convenient since it will allow cancelation of the projection factor in the unit solid angle. The approximation is a rough one, but is certainly an underestimate of the influence of the bank beam upon the integration over the sidelobes of the bandwidth/time response. Hence the resulting contributions of the sidelobes will be overestimated in this approximation.

With the preceding approximations, the two integrals to be evaluated become:

a) $\int B(\ell)d\ell \int B(m)dm$

and b) $\int B^2(\ell)d\ell / B^2(m)dm$.

The formal limits of the integrations are -1 to 1, but in view of the rapid convergence of the integrals due to the large values of C_1 and C_2, extending the integration to infinity causes negligible error. (This means that nearly all of the contribution to the integrals occurs within a few cycles of the sinc and sinc^2 function from the zenith). Evaluation of the integrals gives:

$$\pi^2/C_1C_2$$

for both.

In order to estimate the contribution of the sidelobes versus that from the main beam, we must perform the integrations over these areas separately. Defining the main beam as that region within the first zero-crossing of the sinc function, the integrations give:

a) Beam integral:

1) Main beam: $13.7/C_1C_2$.

b) Beam squared integral:

1) Main beam: $8.07/C_1C_2$

2) Sidelobes: $1.80/C_1C_2$.

(The sidelobe beam integral is not needed).

The function C_1C_2 can easily be converted into more useful units. Expressing frequency and bandwidth in MHz, baseline lengths in kilometers, and time in seconds gives $C_1C_2 = 8.08\times10^{-3}B_M\nu_M L_k^2 t$.

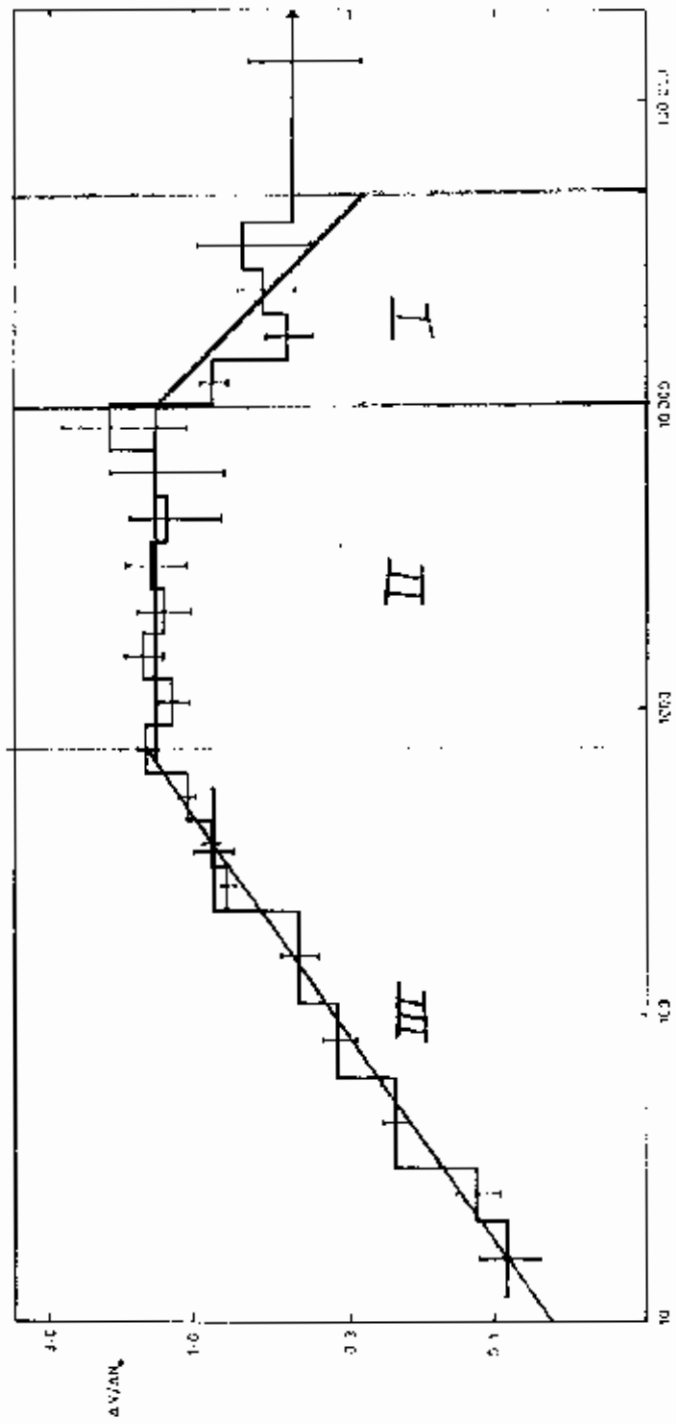

FIG. 5. *Combined differential source counts from* 5C 5, 5C 2 *and Mills et al.* (1973; *i.e. the Molonglo MC*1 *survey for* $220 \leqslant S_{408} < 10\,000 \times 10^{-26}$ *W m*$^{-2}$ *Hz*$^{-1}$, *and a whole-sky compilation for* $S_{408} \geqslant 10^{25}$ *W m*$^{-2}$ *Hz*$^{-1}$). *The normalization is to* $N_0 = 750$ *sr*$^{-1}$ $(S/10^{-25}$ *W m*$^{-2}$ *Hz*$^{-1})^{-1.5}$ *but note that in this Figure the flux densities are on the scale of Wyllie so that both flux densities and normalization differ from those of Fig.* 4(*a*). *The lowest flux density range* ($12{\cdot}0 \leqslant S_{408} < 21{\cdot}3 \times 10^{-29}$ *W m*$^{-2}$ *Hz*$^{-1}$) *includes only the* 5C 5 *sources.*

Fig A-1 Normalised Number Counts at 408 MHz

T. J. Pearson, MNRAS 171, 475 (1975)